

## Article

# Experimental and Numerical Performance Evaluation of Bio-Based and Recycled Thermal Break Strips in LSF Partition Walls

Paulo Santos , David Abrantes, Paulo Lopes  and Diogo Mateus

ISISE, Department of Civil Engineering, University of Coimbra, 3030-788 Coimbra, Portugal

\* Correspondence: pfsantos@dec.uc.pt

**Abstract:** The thermal performance of Lightweight Steel Framed (LSF) walls could be strongly compromised due to steel's high thermal conductivity and their related thermal bridges. In this paper, the performance of bio-based (pine wood) and recycled (rubber–cork composite) Thermal Break Strip (TBS) materials, to mitigate the thermal bridge effect originated by steel profiles in LSF partition walls, is evaluated. This assessment was achieved by measurements under controlled laboratory conditions and by predictions using some numerical simulation models. Regarding the measurements, two climatic chambers (cold and hot) were used to impose a nearly constant temperature difference (around 35 °C), between the LSF partition test samples' surfaces. To measure the overall surface-to-surface thermal resistance (*R*-value) of the evaluated LSF wall configurations, the Heat Flow Meter (HFM) method was used. Moreover, the measured values were compared with the calculations by 2D (THERM models) and 3D (ANSYS models) numerical simulations, exhibiting an excellent agreement (less than  $\pm 2\%$  difference). Three TBS locations and three materials are evaluated, with their thermal performance improvement compared with a reference interior partition LSF wall, having no TBS. The top performance was accomplished by the aerogel super-insulating TBS material. The bio-based material (pine wood) and the recycled rubber–cork composite present quite similar results, with a slight advantage for the pine wood TBSs, given their higher thickness. Considering the TBS location, the inner and outer side present comparable performances. When using TBSs on both sides of steel profile flanges, there is a relevant thermal performance improvement, as expected. The thickness of the TBS also presents a noteworthy influence on the LSF partition thermal resistance.

**Keywords:** lightweight steel frame; thermal break strips; partition walls; bio-based material; measurements; numerical simulations; thermal performance



**Citation:** Santos, P.; Abrantes, D.; Lopes, P.; Mateus, D. Experimental and Numerical Performance Evaluation of Bio-Based and Recycled Thermal Break Strips in LSF Partition Walls. *Buildings* **2022**, *12*, 1237. <https://doi.org/10.3390/buildings12081237>

Academic Editor: Cinzia Buratti

Received: 23 July 2022

Accepted: 11 August 2022

Published: 14 August 2022

**Publisher's Note:** MDPI stays neutral with regard to jurisdictional claims in published maps and institutional affiliations.



**Copyright:** © 2022 by the authors. Licensee MDPI, Basel, Switzerland. This article is an open access article distributed under the terms and conditions of the Creative Commons Attribution (CC BY) license (<https://creativecommons.org/licenses/by/4.0/>).

## 1. Introduction

Climate change, global warming, as well as shortages and high price of fossil fuels, have led to a growing concern and demand regarding energy efficiency, particularly in buildings. This sector consumes nearly forty percent of the total energy in Europe and accounts for approximately 36% of the CO<sub>2</sub> emissions [1]. Improvements of buildings' energy efficiency leads to reduced energy consumption, reduced CO<sub>2</sub> emissions, and also decreasing costs during the operational phase. Energy efficiency and thermal comfort in buildings could be mostly influenced by the physical properties (e.g., thermal resistance) of the building envelope. To reduce CO<sub>2</sub> emissions, the use of biomaterials and recycled materials should be prioritized. The construction sector has been experiencing a change in constructive technology, turning to more lightweight and industrialized alternatives.

The Light Steel Framing (LSF) constructive system is one of these technologies, that has been proliferating due to its advantages compared to the heavyweight reinforced concrete and brick masonry systems, such as: light weight, facilitating transportation and handling; high mechanical strength; easy prefabrication ensuring better quality controlled building components, as well as permitting modular construction; faster construction resulting

in time savings; a more sustainable construction due to its potential of recyclability and reuse, which can exceed 95%; in case of humidity, excellent stability of shape; decrease in waste; reduced water consumption; and less need for heavy machinery and an intensive workforce [2–4].

Regarding Lightweight Steel Framed (LSF) walls, the high thermal conductivity of steel may originate important thermal bridges, that should be predicted in the building design phase and treated at the construction stage [5]. These thermal bridges can reduce the building energy efficiency by more than 30%. Thermal Break Strips (TBSs), an Exterior Thermal Insulation Composite System (ETICS), and slotted steel studs are some of the thermal mitigation strategies usually used in LSF buildings.

Usually, an LSF wall is made of three main constituents: (1) cold formed steel internal frame; (2) sheathing panels on internal side of walls and ceilings (e.g., gypsum plasterboard) and on external side (e.g., Oriented Strand Board—OSB); and (3) insulation materials (air cavity insulation, e.g., mineral wool, and/or Exterior Thermal Insulation Composite System—ETICS) [6,7]. The mineral wool placed inside the air cavity, in addition to the thermal insulation role, causes an important acoustic performance improvement as well, increasing the noise insulation [8,9]. Moreover, the thermal insulation effectiveness is significantly related to the position in the LSF walls [10,11] and the LSF construction type [12].

Indeed, the type of LSF construction system is defined by the presence of the insulation layer and its location on the wall, that can be categorized in three typologies: (1) warm, (2) cold, and (3) hybrid steel frame. In warm frame construction, all insulation is continuous, being positioned on the exterior side of the wall (e.g., ETICS). In cold frame construction, all insulation is located inside the air gap (between the metallic profiles), with their thickness limited to the steel profile depth. Given its usual best thermal performance, the hybrid steel frame type is the most commonly used [8]. In this LSF system, both kinds of insulation are used, namely external continuous, as well as discontinuous batt insulation placed between steel studs [13].

There are three main methodologies to assess the thermal transmittance ( $U$ -value) and/or thermal resistance ( $R$ -value) of building elements: (1) analytical formula computations, (2) numerical simulations, and (3) experimental measurements [14].

Concerning the analytical formulas, they are the simplest method of those mentioned above, being very useful and effortless to be used at the early design stage [15,16]. However, these analytical formulas can only be used, and are available, for very simplified wall arrangements, so their use very restricted. Additionally, these formulations commonly assume a basic one-dimensional (1D) steady-state heat flow and neglect the materials' heat storage effect and/or the variation in thermal properties (e.g., thermal conductivity change with humidity and temperature) [17].

Regarding numerical simulations, the fastest and easiest ones are provided by two-dimensional (2D) models [10,12,18], while the more time-consuming and complete are the three-dimensional (3D) models [19–21]. Notice that this numerical simulation approach has the benefit of permitting a fast comparison among several building element configurations, saving time and money, in comparison with an experimental approach. However, there is a need for a specific and adequate calculation tool (software). To verify their algorithms' reliability, the computed results must be verified using, for instance, the test cases prescribed in standard ISO 10211 [22]. Moreover, to validate the implemented numerical model, the calculated results should be verified by comparison with experimental measurements. These measurements could be carried out in laboratory-controlled conditions or in situ [23,24]. Some often used measurement methods are: Infrared Thermography (IRT); the Hot Box (HB) method, that can be Guarded HB (GHB) or Calibrated HB (CHB); the Heat Flow Meter (HFM) method; and the Guarded Hot Plate (GHP) method [23].

To improve the thermal performance of LSF buildings, several thermal bridge mitigation techniques could be used, such as: flange stud indentation [25,26]; slotted thermal steel studs [19,27,28]; Thermal Break Strips (TBSs) along the steel flanges [12,28,29]; external

continuous thermal insulation (e.g., ETICS) [14,30–32]. Another approach to increase the performance of an LSF element, when there is a cavity inside the wall, is by decreasing the radiation heat transfer. With this purpose, a reflective aluminum foil or a paint having low emissivity inside the LSF wall air gap could be used [33–36]. Regarding the use of TBSs in LSF walls, no study was found in the literature using a bio-based material with this purpose.

In this research work, the thermal performance of bio-based (pine wood) and recycled (rubber–cork composite) materials, used as Thermal Break Strips (TBSs) in LSF partition walls, is evaluated using experimental and numerical approaches. Thus, the surface-to-surface  $R$ -value of LSF partition walls, using different configurations, was assessed under controlled laboratory conditions. The main advantage of using these conductive  $R$ -values is that they do not depend on the surrounding environmental conditions. Therefore, any surface thermal resistance value could be added to obtain the total thermal resistance of the LSF wall.

These laboratory measurements were completed using a set of two climatic chambers (one cold and the other hot). The experimental tests were performed using the HFM method [37]. Moreover, three tests were carried out for each wall, placing the sensors at different locations (bottom, middle, and top), on the surfaces of the LSF wall prototype, corresponding to a total of 30 laboratory tests. Besides the previous bio-based and eco-friendly recycled TBS materials, a high-performance state-of-the-art insulation material (aerogel) was also evaluated. These TBS materials were used on three different LSF wall positions: outer flange, inner flange, as well as on the two steel flanges. Moreover, the measured values were matched with the predictions obtained by 2D (THERM models [38]) and 3D (ANSYS models [39]) numerical simulations, exhibiting an excellent agreement (up to  $\pm 2\%$  difference).

This manuscript is organized as follows. After this brief introductory section, the material and methods are described, including the evaluated LSF partition walls, the laboratory measurements, and the numerical simulations. Next, the obtained results are presented and discussed, namely the conductive thermal resistances, the Infrared (IR) images, and the heat flux predictions. Finally, some concluding remarks about this study are provided.

## 2. Materials and Methods

### 2.1. Description of LSF Partitions

The description of the dimensions, geometry, materials, and thermophysical properties of the LSF reference wall and the Thermal Break Strips (TBSs) is presented in this section. The reference LSF wall corresponds to an LSF wall configuration used as an internal partition. As displayed in Figure 1, this reference LSF partition wall is 140 mm thick, where the inner and outer sheathing surfaces are made of 2 Gypsum Plaster Boards (GPBs) (12.5 mm thick) on each lateral side of the vertical metallic studs ( $C90 \times 37 \times 5 \times 0.6$  mm) spaced 400 mm apart, with the air gap entirely occupied with Mineral Wool (MW) thermal insulation (90 mm thick). Two sheathing drywall layers were adopted to improve the mechanical resistance, as well as to slightly decrease the steel frame thermal bridge effect. In Table 1 are presented the thermal conductivity and thickness values of the materials that make up the reference partition LSF wall.

The TB strips analyzed have a nominal thickness equal to 10 mm and are 50 mm wide. Figure 2 illustrates the materials used, namely Pine Wood (PW), Aerogel (AG), recycled Rubber and Cork (RC) composite. Notice that the thickness of PW strips is slightly higher (13 mm), than the nominal thickness (10 mm). In Table 2 are displayed the thermal conductivities for the TBS materials, changing from 130 mW/(m·K) for PW, down to 15 mW/(m·K) for AG. As shown in Figure 3, the TBSs are placed in three different configuration positions along both steel stud flanges; the inner flange; and the outer flange.

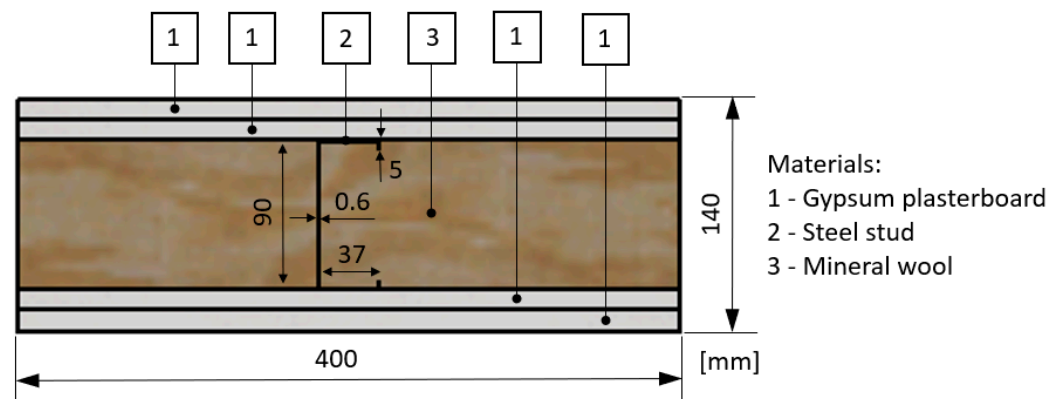


**Figure 1.** Materials, dimensions, and geometry of the reference LSF partition cross-section.

**Table 1.** Thicknesses ( $d$ ) and thermal conductivities ( $\lambda$ ) of materials used in the reference LSF partition wall.

Constitutive Materials	$d$ [mm]	$\lambda$ [W/(m·K)]	Ref.
Gypsum Plaster Board (2 × 12.5 mm)	25	0.175	[40]
Mineral Wool (MW)	90	0.035	[41]
Steel Studs (C90 × 37 × 5 × 0.6 mm)	—	50.000	[42]
Gypsum Plaster Board (2 × 12.5 mm)	25	0.175	[40]
<b>Global Thickness</b>	<b>140</b>	—	—



(a) Pine Wood (PW)



(b) Rubber-Cork (RC)



(c) Aerogel (AG)

**Figure 2.** Thermal break strip materials assembled on the LSF partitions.

**Table 2.** Thermal conductivities ( $\lambda$ ) of the thermal break strips.

Materials (Abbreviation)	$\lambda$ [mW/(m·K)]	Ref.
Pine Wood (PW)	130	[42]
Rubber and Cork composite (RC)	88	[43]
Aerogel (AG)	15	[44]

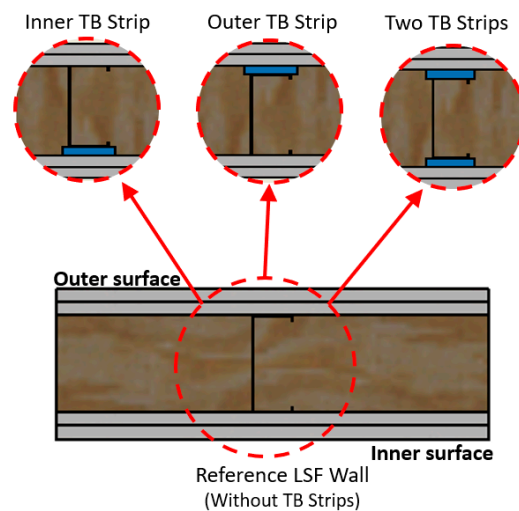
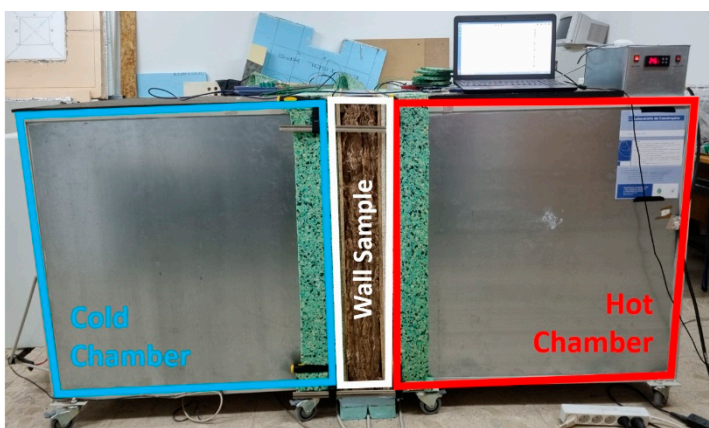


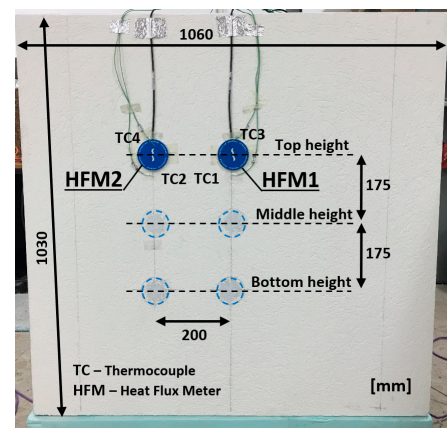
**Figure 3.** Positionings of the Thermal Break Strips (TBSs).

## 2.2. Lab Measurements

The lab measurements were achieved with the aid of a mini hot box apparatus, where the wall prototype is set in the middle of two climatic chambers (cold and hot), as shown in Figure 4a. Notice that, even though not being illustrated in Figure 4a, the perimeter of the wall sample was insulated using a 80 mm layer of polyurethane foam, having a thermal conductivity equal to  $36 \text{ mW}/(\text{m}\cdot\text{K})$ , mitigating the heat losses through the LSF wall test sample perimeter. The cold chamber was cooled by a refrigerator and the hot chamber was warmed up by an electrical resistance of 70 watts. The tested wall samples are 1060 mm wide and 1030 mm high, with a structure composed of three vertical steel profiles, which were set 400 mm apart, where the central one is in the middle.



**(a)** Cold and hot chambers



**(b)** Wall surface sensor location

**Figure 4.** Experimental lab test illustrations.

In this work, the performance of the LSF wall test samples was obtained by making use of the Heat Flow Meter (HFM) method [37], improved for two HFM sensors, one on each wall surface [23]. Four Hukseflux sensors (model HFP01), with a precision of  $\pm 3\%$ , were used to quantify the heat flux passing across the test sample walls, two on the cold side and the other two on the hot side, reducing the duration needed for the tests and improving the precision of the laboratorial measurements, as recommended by Rasooli and Itard [27]. On both sides (cold and hot), one HFM was placed in the middle of the insulation cavity, while the another one was placed over the centered vertical steel stud, at 3 distinct heights, as displayed in Figure 4b, to assess the thermal behavior in 2 different zones.

The temperature measurements were obtained using 12 Type K (1/0.315) PFA insulated Thermocouples (TCs), having class 1 precision certification. Half of them were placed on the hot side, while the other half on the cold side. Moreover, two TCs were used to measure the air temperature inside both chambers (hot and cold), another two TCs were used to measure the wall surface temperatures near the HFMs, and the remaining two were used to measure the air temperature near the wall surface, as displayed in Figure 4b for the cold partition surface.

The cold and hot chambers were set to maintain an average temperature of 5 °C and 40 °C, respectively. These two climatic chambers were well insulated to minimize surrounding heat losses and to ensure that the lab measurements were taken in a condition of near steady-state heat transmission. Notice that in a real building application context, the walls are exposed to transient conditions with variable temperature differences and are exposed to wind and solar radiation effects. The main advantage of using conductive (or surface-to-surface) thermal resistances to quantify the performance of the LSF walls is that it is possible to add any intended surface thermal resistance to calculate the total thermal resistance (or transmittance) depending on the surrounding environmental conditions.

The temperatures and heat flux quantified during the tests were recorded with the aid of one Pico TC-08<sup>®</sup> data-logger, with an accuracy of ±0.5 °C, on each side of the LSF partition wall. The management of this acquired data was performed with the software PicoLog<sup>®</sup>, version 6.1.10, on a laptop computer connected to the data-loggers.

### 2.3. Numerical Simulations

The adopted Finite Element Method (FEM) software, for the thermal bidimensional numerical simulations, was THERM<sup>®</sup> (version 7.6.1). These simulations only consider a representative cross-section of the LSF walls with a steel stud spacing of 400 mm, as shown before in Figure 1 for the reference LSF partition. The hygrothermal properties for the different materials used in these numerical models are displayed in Tables 1 and 2. Furthermore, the error on the FEM results was limited to 2%, for the numerical models evaluated in this research. The boundary conditions regarding environment air temperatures and the surface film coefficients were defined for each simulation.

The air temperatures for the cold and hot environments were equal to 5 °C and 40 °C, respectively. These are average values measured inside the cold and hot chambers. The surface coefficients of heat transfer or film coefficients,  $h$  [ $W/m^2 \cdot K$ ], of the LSF wall surfaces were set equal to the average values obtained for each test, considering the difference between surface and air temperatures,  $\Delta T$  [K], as well as the superficial heat flux,  $q$  [ $W/m^2$ ], as indicated in the following expression:

$$h = \frac{q}{\Delta T} \quad \left( = \frac{1}{R_s} \right). \quad (1)$$

The thermal resistances of the internal and external surfaces,  $R_{si}$  and  $R_{se}$ , ranged within the conventional values predefined in the standard ISO 6946 [45] for the horizontal heat flux, [0.04, 0.13]  $m^2 \cdot K/W$ .

The verification of the software THERM<sup>®</sup> 2D models' accuracy was also confirmed by comparing with 3D models, which were developed using the software ANSYS<sup>®</sup> (version 19.1). With this purpose, two distinct reference wall models were compared, i.e., with and without steel studs, as displayed in Figure 5. The numerical simulations' boundary conditions of the models are the ones mentioned in the previous paragraph. Figure 5 displays the colored temperature distribution for the reference partition wall models configured in the following software: (a) THERM and (b) ANSYS. As illustrated, the simulated colored temperature distributions of the LSF partition wall are very similar. Additionally, the obtained conductive  $R$ -values are analogous, with a nearly zero percentage difference (i.e., −0.8%).

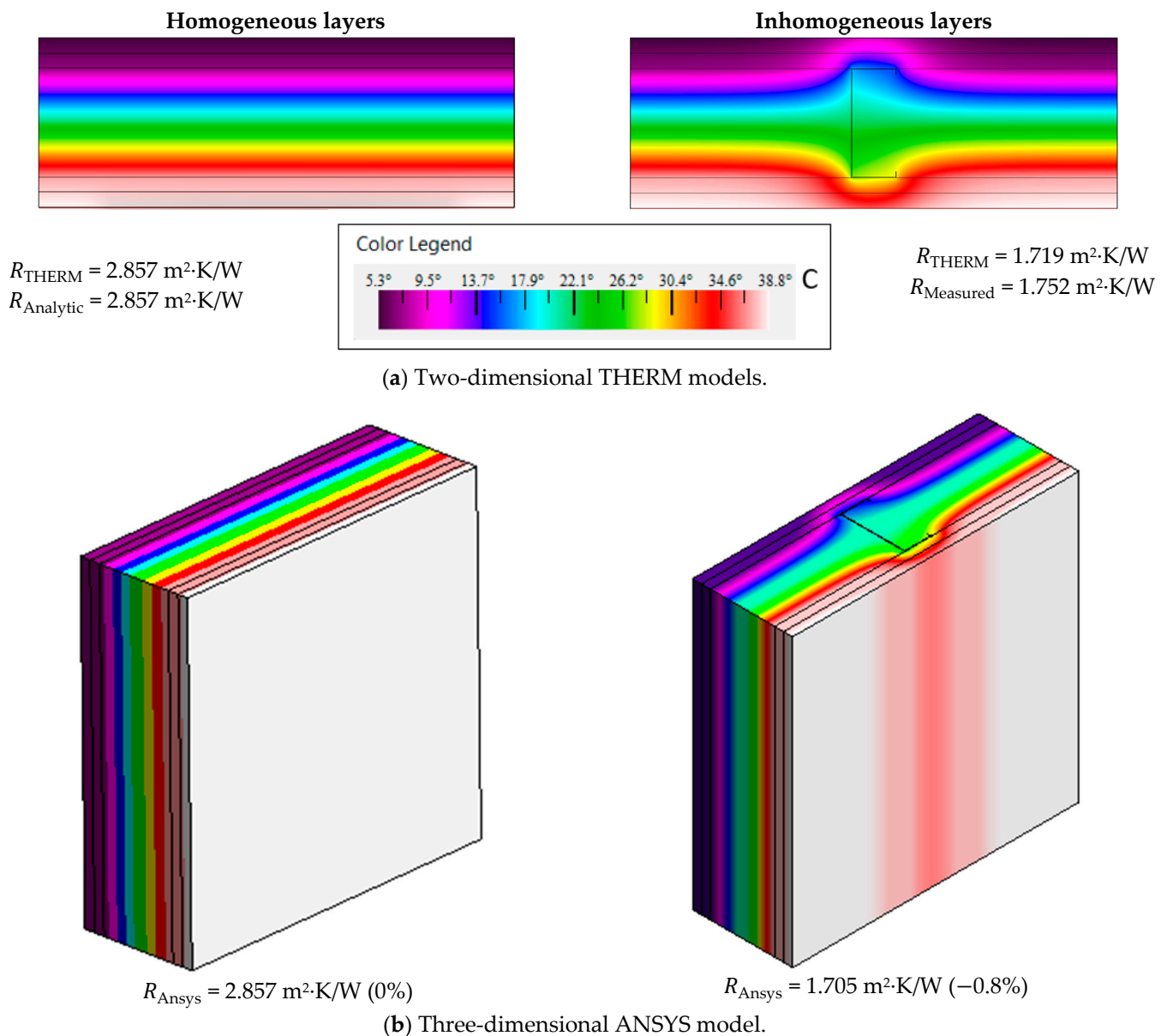


**Figure 5.** THERM models' accuracy: conductive thermal resistances and temperature distribution.

### 3. Results and Discussion

#### 3.1. Conductive Thermal Resistances

In Table 3 are displayed the measured laboratory values and the corresponding computed values by 2D Finite Element Method (FEM) models using the software THERM for the surface-to-surface  $R$ -values of the studied LSF partitions, the percentage and absolute differences among them. The results are divided into four sets: (1) reference LSF partition wall (Ref.); (2) LSF partition walls with an inner TBS ( $PW_{in}$ ,  $RC_{in}$ , and  $AG_{in}$ ); (3) LSF partition walls with an outer TBS ( $PW_{out}$ ,  $RC_{out}$ , and  $AG_{out}$ ); and (4) LSF partition walls with a TBS on two sides, outer and inner ( $PW_{x2}$ ,  $RC_{x2}$ , and  $AG_{x2}$ ).

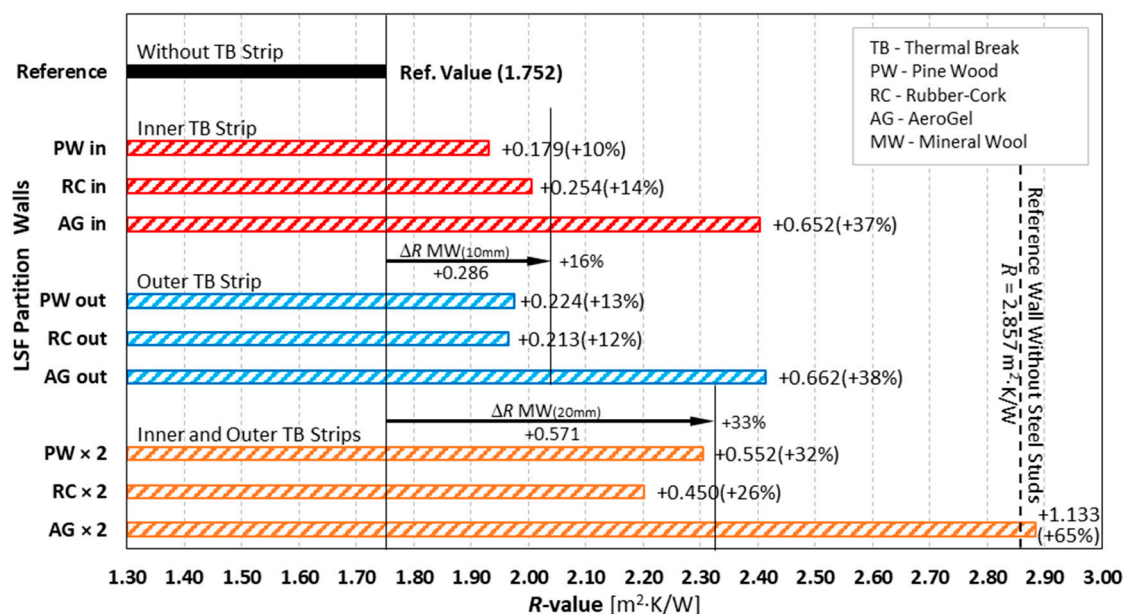
The laboratorial measurements and the numerical predicted  $R$ -values are quite similar, with the biggest differences in percentages being  $\pm 2\%$ . Thus, the accuracy of both computed and measured  $R$ -values is ensured. Moreover, the TBSs can mitigate the heat losses originated by the steel frame thermal bridges, increasing the  $R$ -values of the LSF partitions. This improvement mainly depends on the number of TBSs, their thickness, and material thermal conductivity.

**Table 3.** Numerical (THERM) and experimental (measured) thermal resistances (conductive  $R$ -values).

Wall Code	Wall Description	R-Value		Difference	
		THERM [(m <sup>2</sup> ·K)/W]	Measured [(m <sup>2</sup> ·K)/W]	Absolute [(m <sup>2</sup> ·K)/W]	Percentage [%]
Ref.	Reference LSF Partition Wall	1.719	1.752	+0.033	+2%
PW <sub>in</sub>	Inner Pine Wood TBS	1.976	1.931	−0.045	−2%
RC <sub>in</sub>	Inner Rubber–Cork TBS	2.006	2.006	+0.000	0%
AG <sub>in</sub>	Inner Aerogel TBS	2.359	2.404	+0.045	+2%
PW <sub>out</sub>	Outer Pine Wood TBS	1.981	1.976	−0.005	0%
RC <sub>out</sub>	Outer Rubber–Cork TBS	1.975	1.965	−0.010	−1%
AG <sub>out</sub>	Outer Aerogel TBS	2.358	2.414	+0.056	+2%
PW <sub>x2</sub>	Double Pine Wood TBSs	2.254	2.304	+0.050	+2%
RC <sub>x2</sub>	Double Rubber–Cork TBSs	2.236	2.202	−0.034	−2%
AG <sub>x2</sub>	Double Aerogel TBSs	2.892	2.885	−0.007	0%

TBS—Thermal Break Strip.

In Figure 6, the measured  $R$ -values are graphically displayed, for an easier visualization and comparison. Since the Mineral Wool (MW) batt insulation is expansible, the  $R$ -value rise due to a homogeneous MW layer increment of 10 and 20 mm, equivalent to the thickness of one and two TBSs, respectively, is also displayed.

**Figure 6.** Measured conductive thermal resistances of LSF partition walls.

The thermal conductivity of MW batt insulation (0.035 W/m·K) is lower than Rubber–Cork (RC) composite (0.088 W/m·K) and Pine Wood (PW) (0.130 W/m·K), being higher in relation to Aerogel (AG) (0.015 W/m·K). So, as expected, when using TBS materials with lower thermal conductivities, the thermal performance improvement is lower than the one expected for a homogeneous MW layer. This  $R$ -value increase for a single TBS ranges from +10% up to +14% and for double TBSs from +26% to +32%. However, the  $R$ -values for the LSF partition walls having aerogel TBSs are higher than the expected ones for the homogeneous MW increased layer, with the thermal performance enhancement for these TBSs being equal to: +37% (inner); +38% (outer); and +65% (double TBSs).

Notice that the configuration with aerogel TBSs on both sides of the metallic stud presents a conductive  $R$ -value of 2.885 m<sup>2</sup>·K/W, which means that it fully mitigates the

thermal bridge effect created by the steel frame, since it reaches the  $R$ -value of a homogeneous layered wall without any steel stud, which is  $2.857 \text{ m}^2 \cdot \text{K}/\text{W}$ , as graphically displayed in Figure 6 as a vertical dashed line.

Another interesting and quite surprising feature in Figure 6 is that for the TBSs on the outer flange and with TBSs on both sides of the steel studs, the  $R$ -values measured when using Pine Wood (PW) are higher than when using rubber-cork (RC) composite, even when PW has a higher thermal conductivity ( $0.130 \text{ W}/(\text{m} \cdot \text{K})$ ). This happens since pine wood TBSs, instead of having the nominal 10 mm thickness, are 13 mm thick, which also originates a bigger MW expansion of 3 and 6 mm, for single and double TBSs, respectively.

### 3.2. Thermographic Images

In Figure 7 are illustrated the Infrared (IR) images taken for the tested LSF partition wall cold surface, for the reference wall, and for the LSF partition walls with aerogel TBSs. The purpose was to assess the linear thermal bridge mitigation effect originated by the steel studs' high thermal conductivity. Additionally, in Figure 8 are displayed the profiles for the recorded surface temperatures along the lines (L1 to L4), as presented in Figure 7.

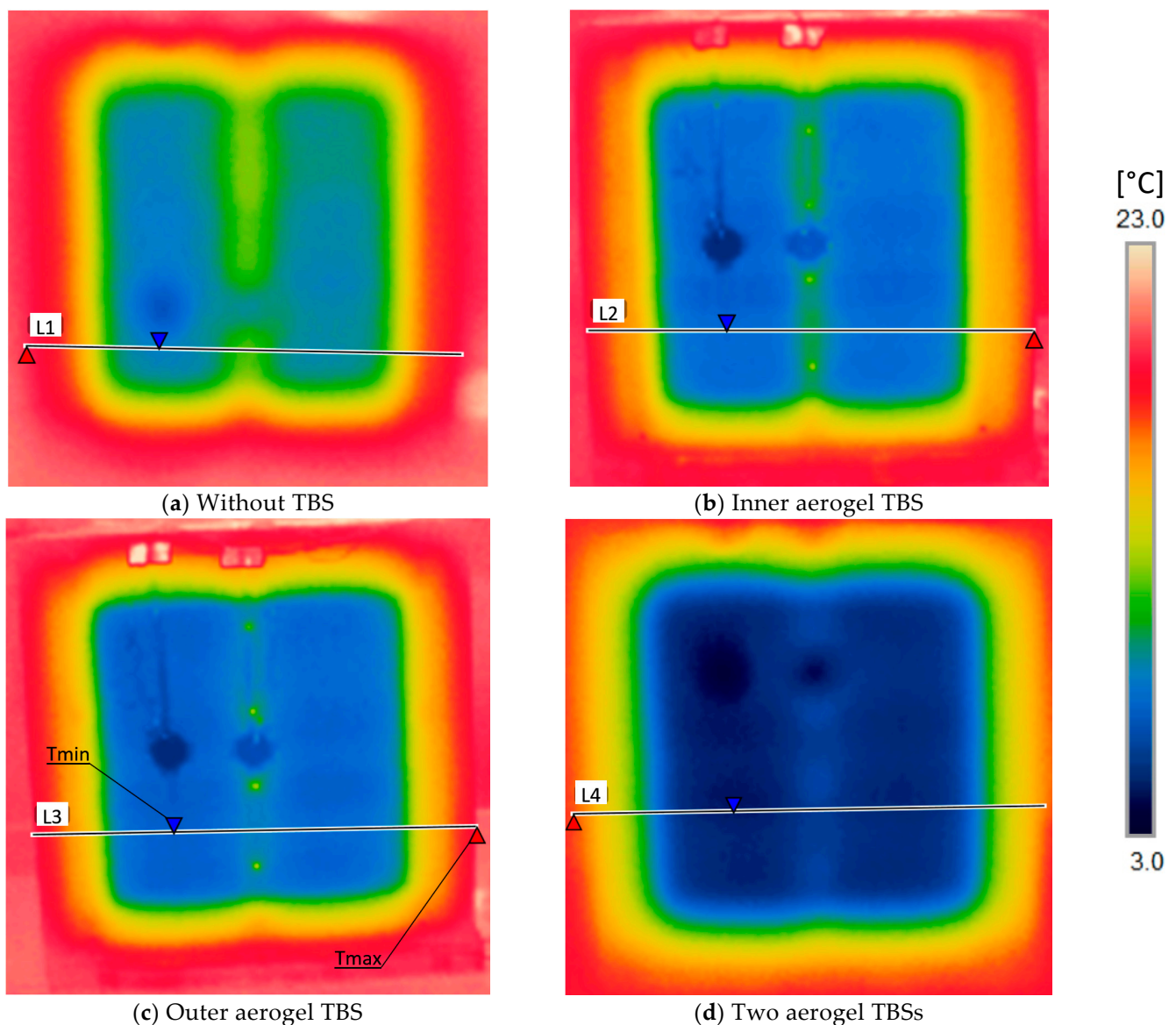
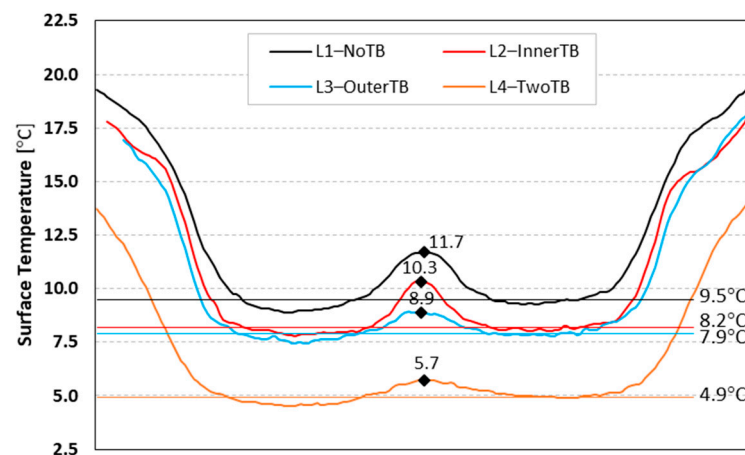


Figure 7. Infrared thermography photos of the LSF partition walls: cold side.



**Figure 8.** Surface temperatures in the four horizontal lines, L1–L4, previously identified in Figure 7.

Looking at the IR images, the vertical steel stud in the center can easily be detected in Figure 7a (LSF partition wall without TBs), due to the increased localized heat transfer, originating a higher surface temperature on the cold surface. In comparison, the central vertical steel stud in Figure 7d is the least pronounced, since the heat transfer for the LSF partition wall with aerogel TBs on both sides of the steel studs is mitigated the most, reducing very significantly the related thermal bridge effect.

Figure 8 also illustrates these features well, where the maximum temperatures are in the central steel profile. In comparison with the average temperature of the wall surface, the differences could be ordered, from higher to lower, as follows: without TBs (L1); with TBs in the interior side flange (L2); with TBs in the outer flange (L3); with TBs in both flanges (L4).

### 3.3. Heat Flux Predictions

A similar assessment was performed using 2D FEM models, computed in THERM, as illustrated in Figure 9, where the predicted heat flux distribution on the cross-section of the four LSF partitions previously illustrated in Figure 7 is displayed.

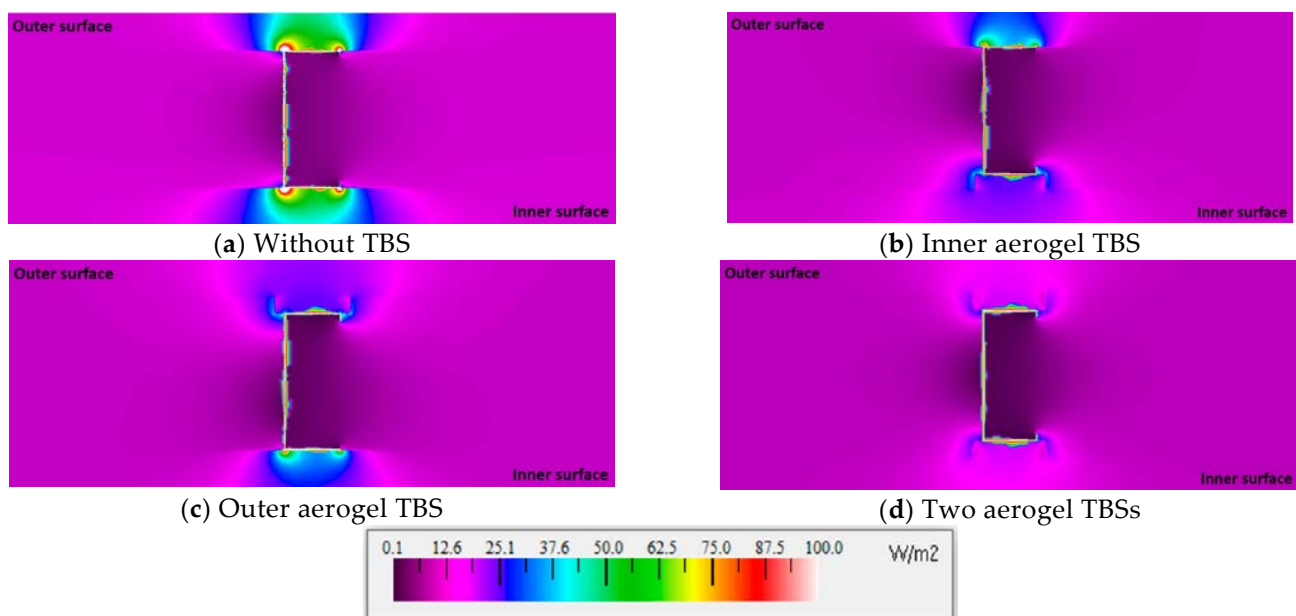


**Figure 9.** Heat flux distribution predicted for the LSF wall cross-sections.

In Figure 9a, there is a higher heat flux near the steel stud flanges, due to the thermal bridge effect. This increased heat flux is related to the higher heat conduction along the steel profile, being more observable near the two sheathing layers on the two sides of the wall, mainly in the vicinity of the metallic flanges, which spreads heat to the gypsum plaster boards. Notice that in the web of the steel stud there is also a significant heat flux, which is not easily visible in this scale. When an aerogel TBS is positioned on the inner (Figure 9b) or outer (Figure 9c) steel flange, the heat flux through the steel flange shows a significant decrease on the TBS side. However, in all the remaining parts the reduction in the heat flux is not as pronounced.

Finally, in Figure 9d the heat flux distribution when a TBS is used on both flanges of the steel profile is illustrated. As expected, the heat flux on both sides of these flanges is highly mitigated, leaving the major heat flux values mainly within the web steel stud. This last illustration allows us to visualize how these two aerogel TBSs can completely attenuate the metallic studs' thermal bridge effect.

#### 4. Conclusions

The performance of Thermal Break Strips (TBSs) on Light Steel Framed (LSF) partitions were measured under quasi-steady-state laboratory conditions. The measured surface-to-surface thermal resistances were compared with the computations provided by Finite Element Method (FEM) simulation models. Several types of TBS materials were tested: (1) a bio-based material (pine wood); (2) an eco-friendly material (recycled rubber–cork composite); and (3) a super-insulation material (aerogel). Moreover, several arrangements regarding the location of the TBS were considered (outer, inner, and on both flanges of the steel studs). For each of the aforementioned configurations, three types of results were analyzed: (1) the measured and the predicted conductive  $R$ -values, for all TBS materials; (2) the recorded temperatures at the cold surface through infrared images, using the super-insulating aerogel TBS; and (3) the THERM predicted heat flux for the same aerogel TBS LSF wall configurations.

Next, we summarize the main achievements of this research work:

- A very good agreement between the  $R$ -value measurements and the numerical simulation predictions was achieved, having differences smaller than  $\pm 2\%$ .
- The thermal performance was quite analogous when a single TBS was utilized on outer or inner steel stud flanges, given the LSF wall symmetry.
- The use of TBSs on both metallic stud flanges significantly enhances the thermal resistance, when compared to the use of only one TBS and without any TBS.
- The best thermal performance was achieved by the aerogel TBS material, given their very reduced thermal conductivity, when compared with the remaining materials.
- The use of the high-performance aerogel TBSs on both steel profile flanges was the unique configuration able to fully mitigate the thermal bridge effect due to the steel frame, reaching the thermal resistance provided by the reference wall having homogeneous layers, i.e., without steel profiles.
- The bio-based pine wood TBS exhibited a better thermal performance when compared to the recycled rubber–cork composite TBS, for some wall configurations (outer and two TBSs).
- The TBSs' thickness also has a significant influence on the wall thermal resistance, not only because it mitigates the local thermal bridge effect on the steel stud, but also given the mineral wool expansion, which increases the wall cavity thermal resistance (between metallic studs).

**Author Contributions:** Conceptualization, P.S. and D.M.; Formal analysis, D.M.; Funding acquisition, P.S.; Investigation, P.S., D.A. and P.L.; Methodology, P.S.; Project administration, P.S.; Resources, P.S. and D.M.; Software, D.A. and P.L.; Supervision, P.S.; Validation, D.A. and P.L.; Visualization, D.A. and P.L.; Writing—original draft, D.A. and P.L.; Writing—review & editing, P.S. and D.M. All authors have read and agreed to the published version of the manuscript.

**Funding:** This research was funded by FEDER funds through the Competitiveness Operational Programme—COMPETE—and by national funds through the Foundation for Science and Technology FCT—within the scope of the project POCI-01-0145-FEDER 032061.

Cofinanciado por: POCI-01-0145-FEDER-032061



**Acknowledgments:** The authors also want to thank the support provided by the following companies: Pertecno, Gyptec Ibéria, Volcalis, Sotinco, Kronospan, Hulkseflux, Hilti, and Metabo.

**Conflicts of Interest:** The authors declare no conflict of interest.

## References

1. EU. Directive (EU) 2018/844 of the European parliament and of the council on the energy performance of buildings and on energy efficiency. *Off. J. Eur. Union* **2018**, *156*, 75–91.
2. Zhan, Q.; Xiao, Y.; Musso, F.; Zhang, L. Assessing the hygrothermal performance of typical lightweight steel-framed wall assemblies in hot-humid climate regions by monitoring and numerical analysis. *Build. Environ.* **2021**, *188*, 107512. [[CrossRef](#)]
3. Soares, N.; Santos, P.; Gervásio, H.; Costa, J.J.; Simões da Silva, L. Energy efficiency and thermal performance of lightweight steel-framed (LSF) construction: A review. *Renew. Sustain. Energy Rev.* **2017**, *78*, 194–209. [[CrossRef](#)]
4. Perera, D.; Upasiri, I.; Poologanathan, K.; Gatheeshgar, P.; Sherlock, P.; Hewavitharana, T.; Suntharalingam, T. Energy performance of fire rated LSF walls under UK climate conditions. *J. Build. Eng.* **2021**, *44*, 03293. [[CrossRef](#)]
5. Ribeiro, T.; Santos, P.; Mateus, D. Performance of Thermal Break Strips in Lightweight Steel Framed Walls. In Proceedings of the 1st International Conference on Water Energy Food and Sustainability (ICoWEFS 2021), Leiria, Portugal, 10–12 May 2021; Springer International Publishing: Cham, Switzerland, 2021; pp. 382–389. [[CrossRef](#)]
6. Santos, P. Chapter 3-Energy Efficiency of Lightweight Steel-Framed Buildings. In *Energy Efficient Buildings*; Yap, E.H., Ed.; InTech: London, UK, 2017; pp. 35–60. [[CrossRef](#)]
7. Silvestre, N.; Pires, J.; Santos, A. *Manual de Conceção de Estruturas e Edifícios em LSF-Light Steel Framing, 1a*; CMM: Coimbra, Portugal, 2013.
8. Roque, E.; Santos, P.; Pereira, A. Thermal and sound insulation of lightweight steel-framed façade walls. *Sci. Technol. Built Environ.* **2019**, *25*, 156–176. [[CrossRef](#)]
9. Wang, C.; Mynors, D. Acoustic performance of cold-formed steel buildings. In *Recent Trends in Cold-Formed Steel Construction*; Woodhead Publishing: Sawston, UK, 2016; pp. 173–182. [[CrossRef](#)]
10. Roque, E.; Santos, P. The effectiveness of thermal insulation in lightweight steel-framed walls with respect to its position. *Buildings* **2017**, *7*, 13. [[CrossRef](#)]
11. Atsonios, I.A.; Mandilaras, I.D.; Kontogeorgos, D.A.; Founti, M.A. Two new methods for the in-situ measurement of the overall thermal transmittance of cold frame lightweight steel-framed walls. *Energy Build.* **2018**, *170*, 183–194. [[CrossRef](#)]
12. Santos, P.; Lemes, G.; Mateus, D. Thermal transmittance of internal partition and external facade LSF walls: A parametric study. *Energies* **2019**, *12*, 2671. [[CrossRef](#)]
13. Santos, P.; Simões da Silva, L.; Ungureanu, V. *Energy Efficiency of Light-Weight Steel-Framed Buildings*, 1st ed.; Technical Committee 14-Sustainability & Eco-Efficiency of Steel Construction; European Convention for Constructional Steelwork (ECCS): Brussels, Belgium, 2012; ISBN 978-92-9147-105-8.
14. Santos, P.; Gonçalves, M.; Martins, C.; Soares, N.; Costa, J.J. Thermal transmittance of lightweight steel framed walls: Experimental versus numerical and analytical approaches. *J. Build. Eng.* **2019**, *25*, 100776. [[CrossRef](#)]
15. Gorgolewski, M. Developing a simplified method of calculating U-values in light steel framing. *Build. Environ.* **2007**, *42*, 230–236. [[CrossRef](#)]
16. Kosny, J.; Christian, J.E.; Barbour, J.; Goodrow, J. *Thermal Performance of Steel Framed Walls*; ORNL Report; Oak Ridge National Laboratory: Oak Ridge, TN, USA, 1994.
17. ASHRAE. *Handbook of Fundamentals*, SI ed.; ASHRAE-American Society of Heating, Refrigerating and Air-Conditioning Engineers: Atlanta, GA, USA, 2017.
18. Muzzi, T.A.; Souza, H.A.; Gomes, A.P. Heat transfer analysis of the vertical closing system in light steel framing using the isothermal planes method and finite element method. *REM-Int. Eng. J.* **2021**, *74*, 425–431. [[CrossRef](#)]
19. Martins, C.; Santos, P.; Simoesdasilva, L. Lightweight steel-framed thermal bridges mitigation strategies: A parametric study. *J. Build. Phys.* **2016**, *39*, 342–372. [[CrossRef](#)]
20. Santos, P.; Martins, C.; Simoesdasilva, L.; Bragança, L. Thermal performance of lightweight steel framed wall: The importance of flanking thermal losses. *J. Build. Phys.* **2014**, *38*, 81–98. [[CrossRef](#)]
21. Manzan, M.; De Zorzi, E.Z.; Lorenzi, W. Numerical simulation and sensitivity analysis of a steel framed internal insulation system. *Energy Build.* **2018**, *158*, 1703–1710. [[CrossRef](#)]

22. ISO 10211; Thermal Bridges in Building Construction-Heat Flows and Surface Temperatures-Detailed Calculations. ISO-International Organization for Standardization: Geneva, Switzerland, 2017.
23. Soares, N.; Martins, C.; Gonçalves, M.; Santos, P.; da Silva, L.S.; Costa, J.J. Laboratory and in-situ non-destructive methods to evaluate the thermal transmittance and behavior of walls, windows, and construction elements with innovative materials: A review. *Energy Build.* **2019**, *182*, 88–110. [[CrossRef](#)]
24. Gori, V.; Marincioni, V.; Biddulph, P.; Elwell, C.A. Inferring the thermal resistance and effective thermal mass distribution of a wall from in situ measurements to characterise heat transfer at both the interior and exterior surfaces. *Energy Build.* **2017**, *135*, 398–409. [[CrossRef](#)]
25. Santos, P.; Poologanathan, K. The importance of stud flanges size and shape on the thermal performance of lightweight steel framed walls. *Sustainability* **2021**, *13*, 3970. [[CrossRef](#)]
26. ThermaChannel. Website 'ThermaChannel-Energy-Efficient Steel Framing'. 2018. Available online: [www.thermachannel.com](http://www.thermachannel.com) (accessed on 5 February 2019).
27. Lupan, L.M.; Manea, D.L.; Moga, L.M. Improving Thermal Performance of the Wall Panels Using Slotted Steel Stud Framing. *Procedia Technol.* **2016**, *22*, 351–357. [[CrossRef](#)]
28. Váradi, J.; Toth, E. Thermal Improvement of Lightweight Façades containing Slotted Steel Girders. In Proceedings of the Twelfth International Conference on Civil, Structural and Environmental Engineering Computing, Funchal, Portugal, 1–4 September 2009.
29. Santos, P.; Mateus, D. Experimental assessment of thermal break strips performance in load-bearing and non-load-bearing LSF walls. *J. Build. Eng.* **2020**, *32*, 101693. [[CrossRef](#)]
30. Kapoor, D.R.; Peterman, K.D. Quantification and prediction of the thermal performance of cold-formed steel wall assemblies. *Structures* **2021**, *30*, 305–315. [[CrossRef](#)]
31. Kempton, L.; Kokogiannakis, G.; Green, A.; Cooper, P. Evaluation of thermal bridging mitigation techniques and impact of calculation methods for lightweight steel frame external wall systems. *J. Build. Eng.* **2021**, *43*, 102893. [[CrossRef](#)]
32. Kosny, J.; Christian, J.E. Thermal evaluation of several configurations of insulation and structural materials for some metal stud walls. *Energy Build.* **1995**, *22*, 157–163. [[CrossRef](#)]
33. Santos, P.; Ribeiro, T. Thermal performance improvement of double-pane lightweight steel framed walls using thermal break strips and reflective foils. *Energies* **2021**, *14*, 6927. [[CrossRef](#)]
34. Bruno, R.; Bevilacqua, P.; Ferraro, V.; Arcuri, N. Reflective thermal insulation in non-ventilated air-gaps: Experimental and theoretical evaluations on the global heat transfer coefficient. *Energy Build.* **2021**, *236*, 110769. [[CrossRef](#)]
35. Jelle, B.P.; Kalnaes, S.E.; Gao, T. Low-emissivity materials for building applications: A state-of-the-art review and future research perspectives. *Energy Build.* **2015**, *96*, 329–356. [[CrossRef](#)]
36. Fantucci, S.; Serra, V. Investigating the performance of reflective insulation and low emissivity paints for the energy retrofit of roof attics. *Energy Build.* **2019**, *182*, 300–310. [[CrossRef](#)]
37. ISO 9869-1; Part 1: Heat Flow Meter Method. Thermal Insulation-Building Elements-In-Situ Measurement of Thermal Resistance and Thermal Transmittance. ISO-International Organization for Standardization: Geneva, Switzerland, 2014.
38. THERM. Software Version 7.6.1. Lawrence Berkeley National Laboratory: Berkeley, CA, USA. 2017. Available online: <https://windows.lbl.gov/software/therm> (accessed on 14 February 2019).
39. ANSYS Workbench. Software Version 19.1. ANSYS, Inc.: Canonsburg, PA, USA. 2018. Available online: [www.ansys.com/products/](http://www.ansys.com/products/) (accessed on 8 June 2020).
40. Gyptec, I. Technical Sheet: Standard Gypsum Plasterboard. 2022. Available online: [https://www.gyptec.eu/documentos/Ficha\\_Tecnica\\_Gyptec\\_A.pdf](https://www.gyptec.eu/documentos/Ficha_Tecnica_Gyptec_A.pdf) (accessed on 10 February 2022).
41. Volcalis. Technical Sheet: Alpha Mineral Wool. 2022. Available online: [https://www.volcalis.pt/categoria\\_file\\_docs/fichatecnica\\_volcalis\\_alpharollo-386.pdf](https://www.volcalis.pt/categoria_file_docs/fichatecnica_volcalis_alpharollo-386.pdf) (accessed on 10 February 2022).
42. Santos, C.; Matias, L. *ITE50-Coefficientes de Transmissão Térmica de Elementos da Envolvente dos Edifícios*; LNEC-Laboratório Nacional de Engenharia Civil: Lisboa, Portugal, 2006. (In Portuguese)
43. MS-R0 Test Report. Test Report Ref. 5015 PE 1977/08-Determination of Thermal Conductivity (Acousticork MS-R0). In *Departamento de Engenharia Têxtil*; Universidade do Minho: Braga, Portugal, 2008.
44. Proctor Group. Spacetherm® CBS Specification. 2018. Available online: <https://www.proctorgroup.com/assets/PerformanceSpecs/SpacethermCBSPerformanceSpecification.pdf> (accessed on 10 February 2022).
45. ISO 6946; Building Components and Building Elements—Thermal Resistance and Thermal Transmittance—Calculation Methods. ISO-International Organization for Standardization: Geneva, Switzerland, 2017.